Sixth International Symposium on Marine Propulsors
smp'19, Rome, Italy, May 2019

Comparison between LDA measurements and CFD predictions of a wake behind a frigate hull form and propeller

William Batten, James Alderton, Kim Lake*, Richard Pattenden

QinetiQ, Haslar Marine Technology Park, Gosport, Hampshire, UK

ABSTRACT

This paper compares Laser Doppler Anemometry (LDA) measurements of the wake in the region of the propeller for a twin-shaft frigate hull form with RANS CFD predictions. Three sets of LDA measurements have been made: the nominal wake in the location of the propeller, the averaged wake one third of a diameter downstream of the propeller and unsteady wake rakes upstream and downstream of the propeller. The measurements of the wake rakes are synchronised to shaft speed which allows capture of the transient velocity components during a blade pass. The CFD predictions are performed using STAR-CCM+ on a half domain which includes the tunnel working section and the hull form with all appendages. For the nominal wake comparison a mesh sensitivity study has been performed. The CFD study compares the wake as an implicit, time dependent solution with rigid body motion and a sliding interface for the propeller region. The simulations have been run with the k-ω SST turbulence model and have shown reasonable agreement with both the nominal and averaged wakes.

Keywords

Laser Doppler Anemometry, CFD, RANS, propeller wake, SST *k-ω*

1 INTRODUCTION

Predictions of the nominal wake behind frigate hull forms are performed regularly to inform the propeller design, but challenges exist in predicting the fine details. The nominal wake on a typical twin-shaft frigate is dominated by the boundary layer that has developed along the hull, vortices from sonar dome, bilge keels and stabiliser fins, wake deficits behind the A- and P-brackets, and vortices that form on the top of the shaft itself. The dynamic wake structure behind the propeller is also of interest when looking at the formation of the hub vortex, the design of mitigation devices such as vaned boss caps, and the alignment of the rudder. The interaction between the complex flow field upstream of the propeller and the flow over the propeller itself makes capturing the wake near the hub behind the propeller a complex problem both during experiments and in computational models.

Both the Gothenburg and Tokyo workshops (Larsson et al. 2000, Hino 2005, Larsson 2010) have demonstrated the effects of predicting the wake fields around ship hull forms. These simulations have highlighted several issues of RANS modelling, notably due to the anisotropy of turbulence in the wake of a ship hull form.

CFD validation of wake behind an open water propeller has been studied in various workshops as a part of benchmarking studies (Potsdam, 2011) and comparisons by Starke et al. (2006) and Wang & Walters (2012). These studies have highlighted the importance of mesh refinement and demonstrate significant differences with the choice of turbulence model.

This work presents a validation study comparing Laser Doppler Anemometry (LDA) measurements in a large cavitation tunnel and CFD predictions. The hull form is of a generic frigate with a pair of typical low signature propeller designs.

2 GEOMETRY AND TUNNEL CONDITIONS

2.1 Tunnel conditions

The LDA measurements were performed in the large working section of the Grand Tunnel Hydrodynamique (GTH) at Val De Reuil, France. The tunnel working section has a length of 10 m, width of 2 m and height of 1.35 m with speeds of up to 12 m/s. For the nominal wake survey the tunnel speed was set at 7 m/s. For the wake measurements around the propeller the tunnel speed was 5.75 m/s in order to reduce the loads during the duration of the experiment.

2.2 Hull and propeller model

The LDA measurements have been taken around the region of the propeller in the behind condition. The model hull is a scaled generic frigate hull form bolted to the lid of the tunnel as shown in Figure l. The hull model has a length of almost 8 m and maximum beam of over 1 m. The hull form has all the usual appendages for a frigate hull form; sonar dome, bilge keels, fin stabilizers, A-bracket, shafts and rudders. Both included shafts run parallel to each other and are driven through a pair of dynamotors via a split shaft gearbox and motor drive system.

The propeller model is of a generic 5-bladed low

* Now at Leonardo MW Ltd, Southampton, UK

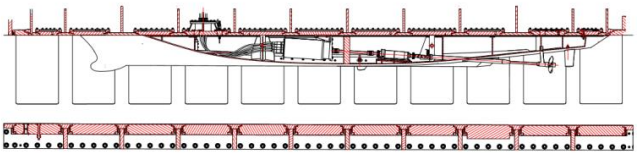

(a) **Profile view**

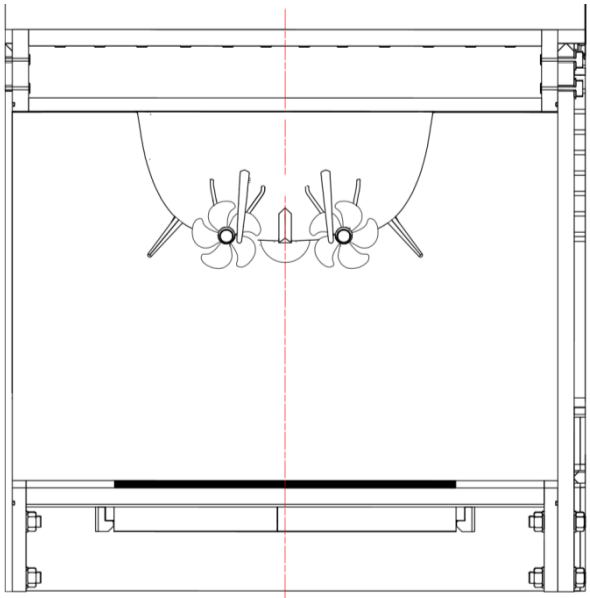

(b) Aft view

Figure 1: Schematics of model test setup in the tunnel

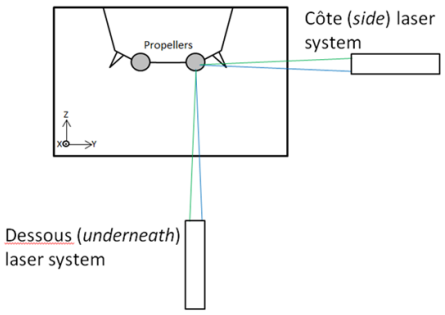

Figure 2: Illustration of LDV system

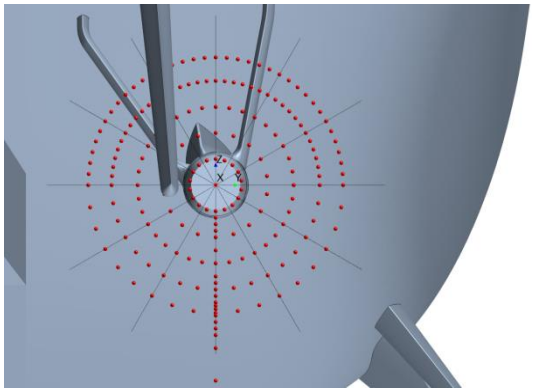

Figure 3: CAD representation of the model showing the location of the measurement points

signature design suitable for the frigate hull form tested. The tunnel speed and RPM were chosen to ensure that the Reynolds number at 0.7 R is over 2 x 10^6. This provided a good balance between synchronised LDA measuring requirements and reducing low Reynolds number boundary layer effects on the propeller blade.

3 EXPERIMENTAL WAKE MEASUREMENT SETUP

3.1 Laser System

The wake survey was performed using the LDA capability at the GTH facility. This LDA system consists of two, independent, two-component LDA probes positioned as shown in Figure 2. The 'Côte' probe, provides measurements in the axial (V_X) - vertical (V_Z) velocity plane. The 'Dessous' probe provides measurements in the axial (V_X) - transverse horizontal (V_Y) velocity plane. Combining these velocity planes gives the full 3D measured velocity.

3.2 Wake locations

Nominal measurements were made as shown in the red points in Figure 3. The angular intervals between these points were 10° at the bottom of the propeller and 5° at the top, where key wake features would be found. The circumferential lines are at a radius of r/R = 0.4, 0.6, 0.8 and 0.98.

The time-averaged propeller wake measurements were taken one third of a diameter downstream of the propeller with the same radial and circumferential locations as the nominal wake measurements.

The measurements of the wake rakes were synchronised to the shaft speed which allowed the capture of the transient velocity components during blade passes. These time histories of velocities were measured along a line at three locations corresponding to axial distances of x/D = 1/4 and 1/3 along the shaft axis downstream of the propeller. The line ranges from a radial position of r/R = 0.2 to 1.5 with varying point density based on the gradient of the flow structures present within the wake.

3.3 Experiment conduct

For the nominal and averaged wake plane, measurements with sample size of 1,000 were taken over a polar grid of measurement positions as detailed in Section 3.2. The choice of 1,000 samples was based on analysis of convergence of the mean at a radius of r/ = 0.6 and the available tank test time.

The transient measurements on the radial wake lines had a sample size of 20,000 and were binned in 5 degree intervals of propeller blade angle. These measurements were taken over the radial line as detailed in Section 3.2. The use of a 5 degree bin size corresponds to around 280 samples for each bin providing a good balance between measurement time for a measurement point and accuracy.

4 CFD WAKE PREDICTIONS

4.1 CFD simulation setup

The CFD analysis was carried out using the commercially available CFD code STAR-CCM+ V12.04. The domain consisted of a symmetrical half model of the GTH tunnel working section, which was extruded upstream and

downstream, parallel to the tunnel lid. The contraction and diffuser sections of the tunnel were not modelled.

4.1.1 Meshing approach

The propeller CAD was segmented, such that only one blade and hub was meshed between a pair of periodic surfaces, using polyhedral cells. The resulting single blade section mesh was then placed in the behind condition simulation, where it was duplicated and fused, resulting in a complete propeller domain. This methodology therefore ensures that each blade is meshed in exactly the same way.

Localised mesh refinement was applied around all regions of interest. The surface mesh of the propeller was refined around the leading and trailing edges of the propeller geometry in order to capture the complex curvature. The boundary layer of the propeller, hull, appendages, and shaft-line were all resolved using prismatic cells. For these boundaries the near-wall cell thickness was defined such that the resulting wall y+ is less than one to ensure the viscous boundary layer is explicitly resolved. The tunnel walls were modelled using a wall function with a y+ set to around one hundred.

4.1.2 Simulation approach

The basic physics setup followed the assumptions:

- Constant fluid density, incompressible flow
- Shear Stress Transport (SST) (Menter, 1994) *k-ω* turbulence model
- All y+ wall treatment models
- Iteration of the inlet velocity to match the velocity at the location of the cavitation tunnel Pitot tube

For the nominal wake simulations a steady-state solution method was used and iterated for over 20,000 iterations. For the nominal wake comparison the velocities were averaged in the same plane as the LDA measurements over the last 2000 iterations.

For the predictions with a propeller wake the solution was initialised using a steady-state solution in which the propeller region was treated as a rotating reference frame. Once the initial converged flow solution was achieved an implicit unsteady time-dependent solution with rigid-body motion of the propeller region was activated. For the first eight rotations the time step was based on a rate of two degrees per time step, after which it was reduced to one degree per time step. For the averaged wake planes behind the propellers the velocities were averaged for the last two rotations (720 time steps).

All presented normalised velocities have been normalised by the tunnel velocity measured at the Pitot tube.

4.2 Nominal wake mesh convergence

The convergence of the mesh was studied by varying the base size of the mesh with a constant near-wall cell size. The results of six changes in mesh size are presented in Figure 4 and Table 1. The uncertainty values presented in Table 1 are calculated using the least-squares regression methodology of Eça et al. (2010).

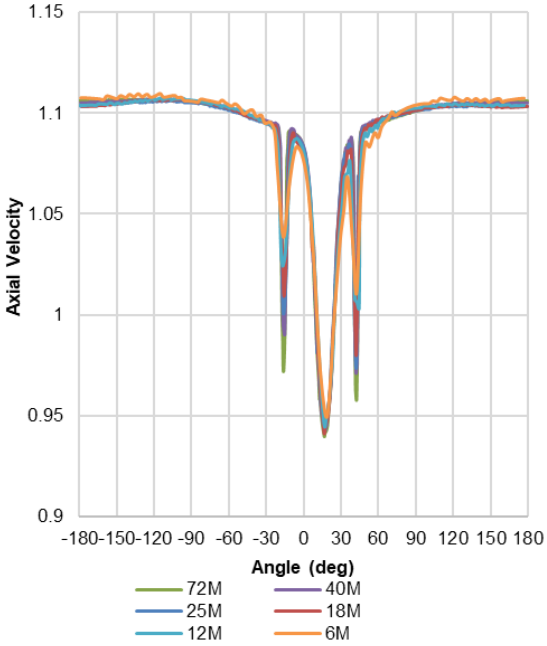

Figure 4: Variation of nominal axial wake for six mesh resolutions at r/R = 0.8

Grid Size	Rudder Resistance [N]	Wake fraction
72M	15.05	1.093
40M	15.30	1.093
25M	15.15	1.091
18M	15.53	1.090
12M	16.50	1.088
6M	18.18	1.089
Uncertainty (25M case)	7.0 %	0.2 %

Table 1 Effect of grid size on solution convergence for nominal wake solution

Inspection of the axial wake in Figure 4 shows similar wake patterns between the six meshes, with the central deficit having a constant value but increasing velocity deficits in the wakes of the A-bracket arms. This illustrates that further localised mesh refinement in these wake regions would be preferable, due to the large cell sizes relative to the wake width.

It is easier to assess grid convergence using integral quantities, so Table 1 shows both the integral wake fraction in the propeller disc and the resistance of the rudder. These show the values converge on finer grids.

As the wake fraction is only changing by a small amount, for the propeller wake study the base size which produced a medium quality grid of 25M cells was chosen as reasonable balance between mesh quality and computational resource.

4.3 Propeller wake convergence

In order to ensure that the solution was converged and time independent, the forces on the propeller blades were monitored for a series of revolutions. These results are shown in Table 2 and show minor changes after halving of time step between the 8th and 9th revolution. The torque

	Thrust (N)	Torque (Nm)
Experiment	418.6	26.3
8th revolution	413.0	26.5
9th revolution	413.1	26.5
10th revolution	413.1	26.5

Table 2: Comparison between thrust and torque between experiment and CFD predictions over an averaged revolution

and thrust values are also very close to the experimental values providing confidence in the simulations. These predictions are however closer than normally found in the literature where RANS solutions without transition model typically over-estimate the torque and under-estimate the thrust (e.g. Wang & Walters, 2012).

The number of additional cells due to the rotating region is approximately 35M. This is considered by the authors to be a medium quality mesh for wake studies. Work is currently ongoing to demonstrate mesh convergence in the region of the propeller domain.

4.4 Typical flow visualisation

Figure 5(a) plots the nominal wake fraction behind the propeller, where a value of one (yellow) represents free-stream ship velocity, less than one (green to blue) represents flow deceleration and above one (red) represents accelerated flow. The wake structures of all appendages are clearly evident. Figure 5(b) shows wake fraction behind the propeller showing the strong flow acceleration behind the propeller.

5 COMPARISON OF WAKE DATA

5.1 Nominal wake

The comparisons of averaged wake results with the measured data for axial, tangential, and radial velocities at different radii are shown in Figures 6, 7 & 8 respectively. The zero degree angle represents top dead centre and positive angles are inboard on the starboard side. Excluding the results at r/R = 0.4 the results demonstrate that the general trends are similar between LDA data and the CFD predictions with similar velocity magnitudes in all three components.

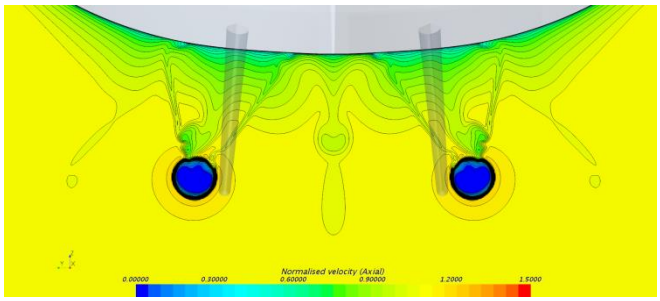

(a) Nominal wake fraction behind the propellers (40M)

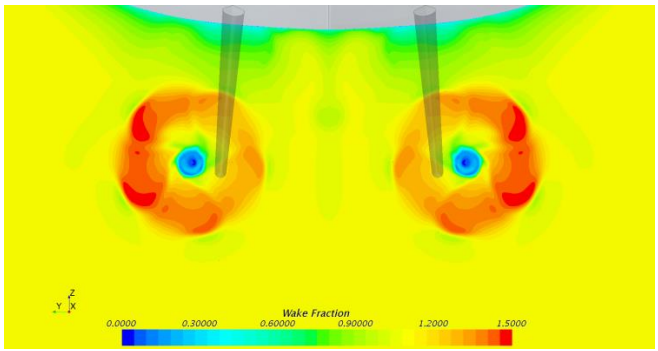

(b) Wake fraction a 1/3 diameter behind the propellers

Figure 5: Typical CFD predicted wake

However, there are clearly regions where there are offsets, highlighting differences in flow details. Figure 6 shows that the CFD prediction tends to have a larger wake deficit in the A-bracket wakes for the outer radii. This could be due to additional secondary flow features that are not modelled due to the choice of turbulence model.

At an angle of 180° the axial velocity under-predicts the LDA measurements this is assumed to be due to the methodology of iterating the inlet velocity to match the Pitot tube measurement without modelling the tunnel contraction.

At r/R = 0.4 the flow is strongly affected by the hub and there a highly unsteady flow due to the flow passing around the rotating shaft and through the A-bracket. Consequently, the level of uncertainty is probably too high draw any firm conclusions in these comparisons.

5.2 Time averaged propeller wake

The comparison of the averaged wake results for axial, tangential and radial velocity at different radii for x/D = 1/3 are shown in Figures 9, 10 & 11 respectively. These results demonstrate that the general trends are in a good agreement between LDA data and the CFD predictions. There are regions where there are offsets highlighting differences in flow details.

At r/R = 0.4 the agreement is better than for the nominal wake. This is assumed to be due to the act of the propeller breaking up the vortex structures.

5.3 Transient propeller wake rake

The transient data has been compared using polar contour plots for axial, radial, and tangential velocities at axial distances of at x/D of 1/4 and 1/3 over a blade pass in Figures 12, to 15. As discussed in the previous paragraphs the general trends between the LDA and CFD results have good agreement. The axial flow shows good agreement in both location and magnitude with the CFD capturing less detail in the wake sheet.

The tangential wake results presented in Figure 14 highlight a lack of detail and low magnitude in the wake for the CFD predictions. This is most likely to be due to insufficient mesh resolution in the wake and tip vortex region. The radial flow wakes presented in Figure 15 show good agreement between r/R = 0.25 and 0.7. However in the tip region the CFD under predicts the magnitude of the velocity components and has less detail. These highlights that the CFD may not be capturing the magnitudes of the tip vortex rotation.

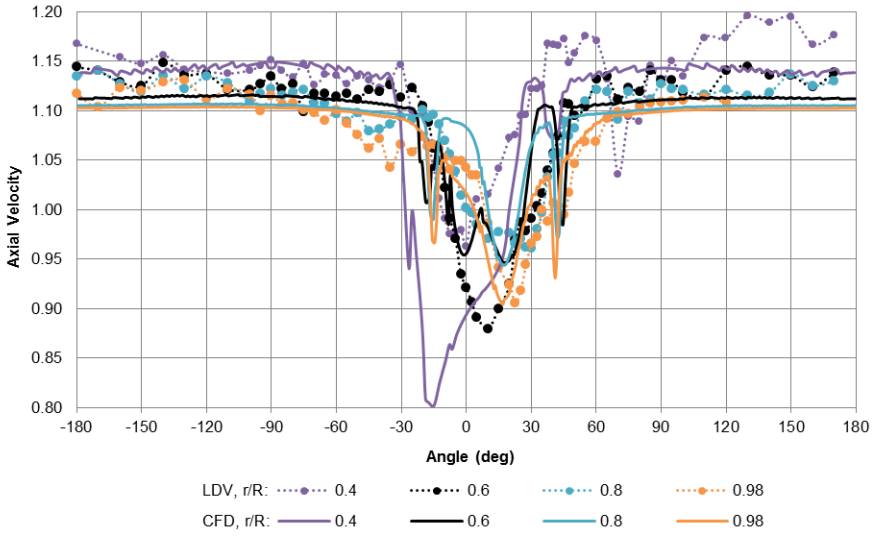

Figure 6: Comparison of the nominal normalised axial velocity component on radii of r/R = 0.4, 0.6, 0.8, and 0.98 at the propeller plane

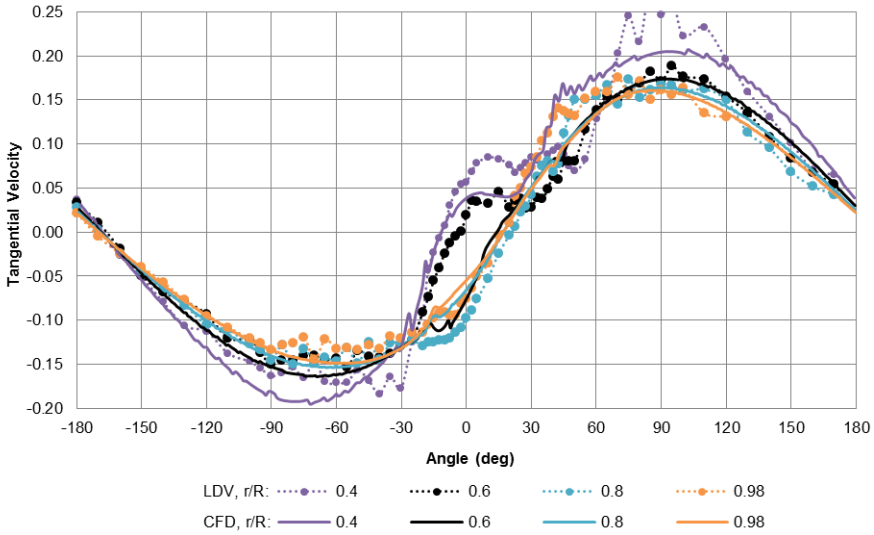

Figure 7: Comparison of the nominal normalised tangential velocity component at radii of r/R = 0.4, 0.6, 0.8, and 0.98 at the propeller plane

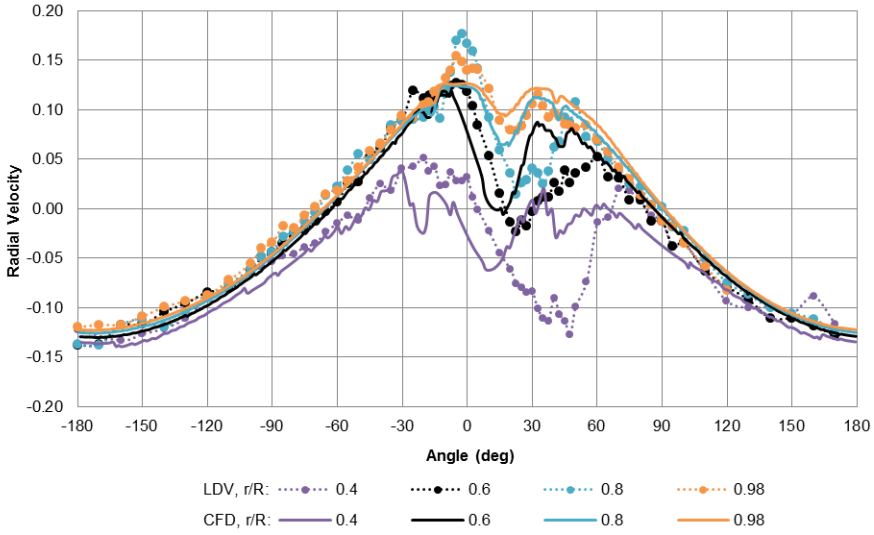

Figure 8: Comparison of the nominal radial velocity component on radii of r/R = 0.4, 0.6, 0.8, and 0.98 at the propeller plane

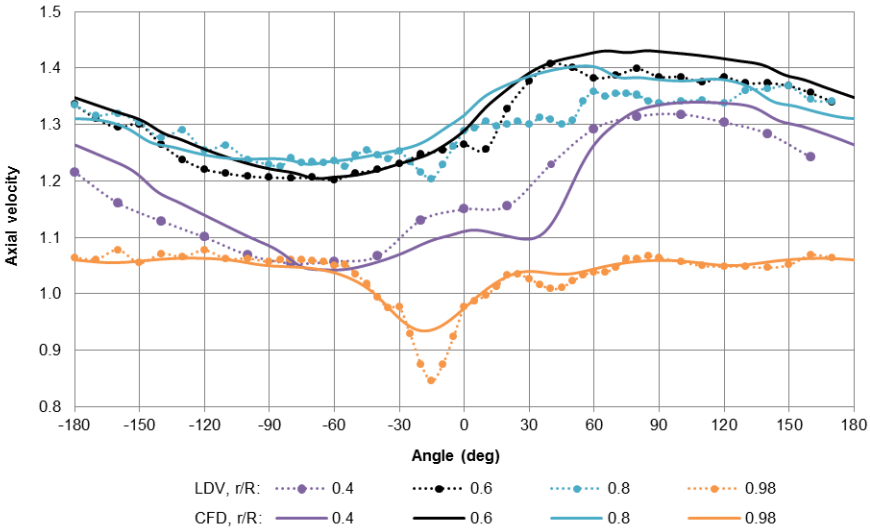

Figure 9: Comparison of averaged normalised axial velocity component on radii of r/R = 0.4, 0.6, 0.8, and 0.98 at axial distance of at x/D = 1/3 downstream of the propeller

6 CONCLUSIONS AND RECOMMENDATIONS

The current approach predicted the torque and thrust to a good level of accuracy. The general predictions of the wake are in line with the LDA measurements although there are some noticeable areas with significant differences.

For the nominal wake measurements the use of the k-ω SST only predicts the key features and magnitudes of the wake. The use of higher order turbulence models with transition models or DES simulations is likely to be required to capture more detail.

For the wake measurements behind the propeller the differences are assumed to be lack of fidelity in the CFD predictions as the transient wake deficits are less than the averaged LDA measurement data set.

Future work is on-going to improve the quality of the CFD predictions. The following three steps are recommended.

1. Reduce the uncertainty in baseline flow in the cavitation tunnel by modelling the contraction and expansion.

2. The use of adaptive meshing should be investigated to allow local refinement of the tip vortices and wake sheets without prior knowledge of their location.

3. Comparisons with DES simulations.

ACKNOWLEDGMENTS

The authors acknowledge the UK MoD for supporting the research and development through the Maritime Strategic Capability Agreement and the use of the GTH through the associated UK/Fr Memorandum Of Understanding on the use of maritime test facilities.

REFERENCES

Starke, B., Windt, J. & Raven, H. (2006). 'Validation of viscous flow and wake field predictions for ships at full scale'. 26th Symposium on Naval Hydrodynamics Rome, ITALY

Eça, L., Vaz, G., & Hoekstra, M. (2010), 'Code verification, solution verification and validation in RANS solvers'. Proceedings of ASME 29th International Conference, OMAE2010, Shanghai, China.

Hino, T. (editor)(2005), 'CFD Workshop Tokyo'. National Maritime Research Institute, Tokyo, Japan.

Larsson, L., Stern, F. and Bertram, V. (eds.)(2000), 'Gothenburg 2000 - A workshop on numerical ship hydrodynamics', Chalmers University, Gothenburg, Sweden.

Larsson, L., Stern, F. and Visonneay, M. (eds.)(2010), 'An assessment of the Gothenburg 2010 Workshop', Numerical Ship Hydrodynamics, Springer, UK.

Menter, F.R. (1994). 'Two-equation eddy-viscosity turbulence models for engineering applications', AIAA Journal, Vol. 32.

Potsdam (2011). "Workshop: Propeller Performance, Potsdam Propeller Test Case (PPTC) LDV Measurements with the Model Propeller VP1304 Case 2.2'. 2nd Symposium on Marine Propulsors, Hamburg, Germany.

Wang, X. & Walters. K. (2012). 'Computational Analysis of Marine-Propeller Performance Using Transition-Sensitive Turbulence Modeling'. ASME: Journal of Fluids Engineering Vol 134.

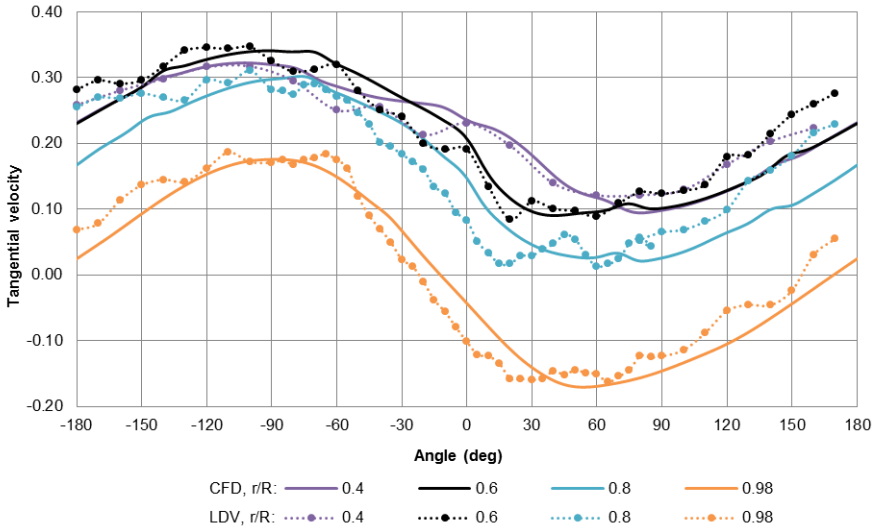

Figure 10: Comparison of averaged normalised tangential velocity component on radii of r/R = 0.4, 0.6, 0.8, and 0.98 at axial distance of at x/D = 1/3 downstream of the propeller

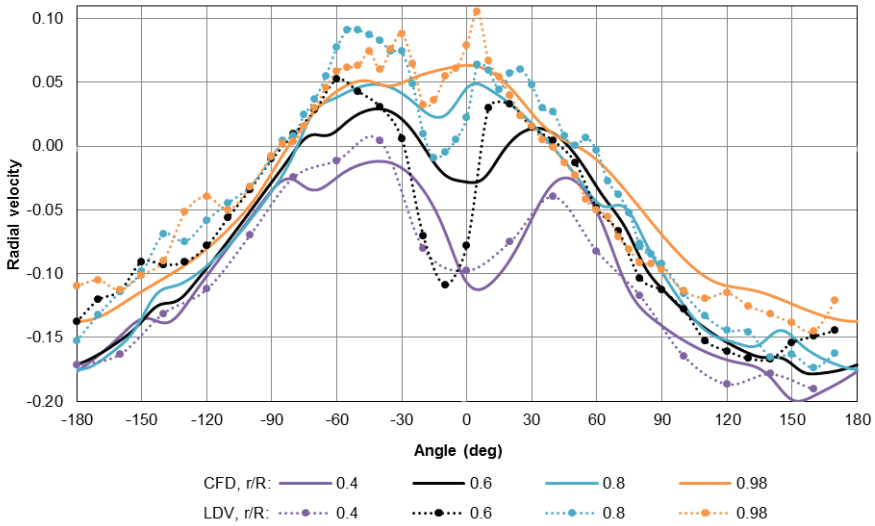

Figure 11: Comparison of averaged normalised radial velocity component on radii of r/R = 0.4, 0.6, 0.8, and 0.98 at axial distance of at x/D = 1/3 downstream of the propeller

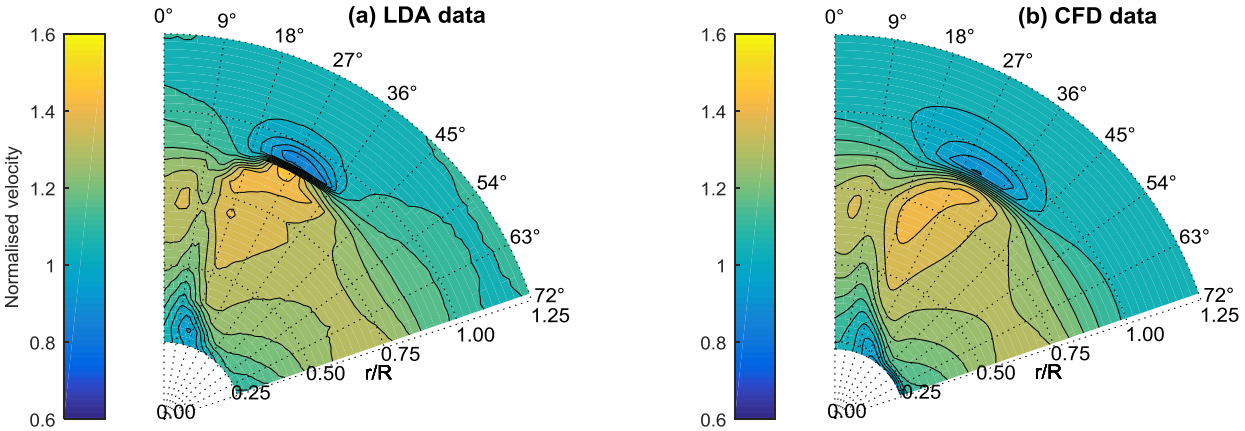

Figure 12: Comparison of polar contour plots of axial velocity component over a blade pass at an axial distance, x/D = 1/4

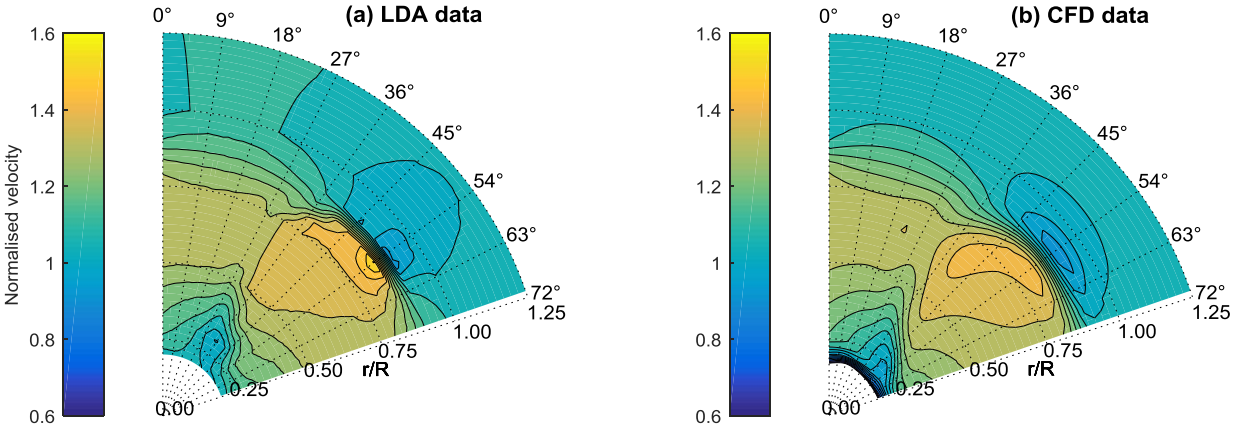

Figure 13: Comparison of polar contour plots of axial velocity component over a blade pass at an axial distance, x/D = 1/3

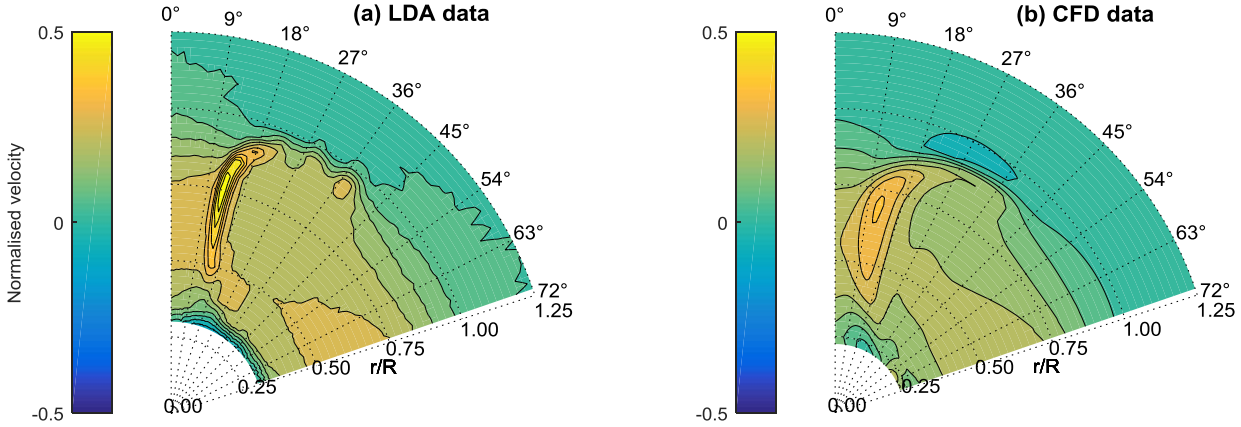

Figure 14: Comparison of polar contour plots of tangential velocity component over a blade pass at an axial distance, x/D = 1/4

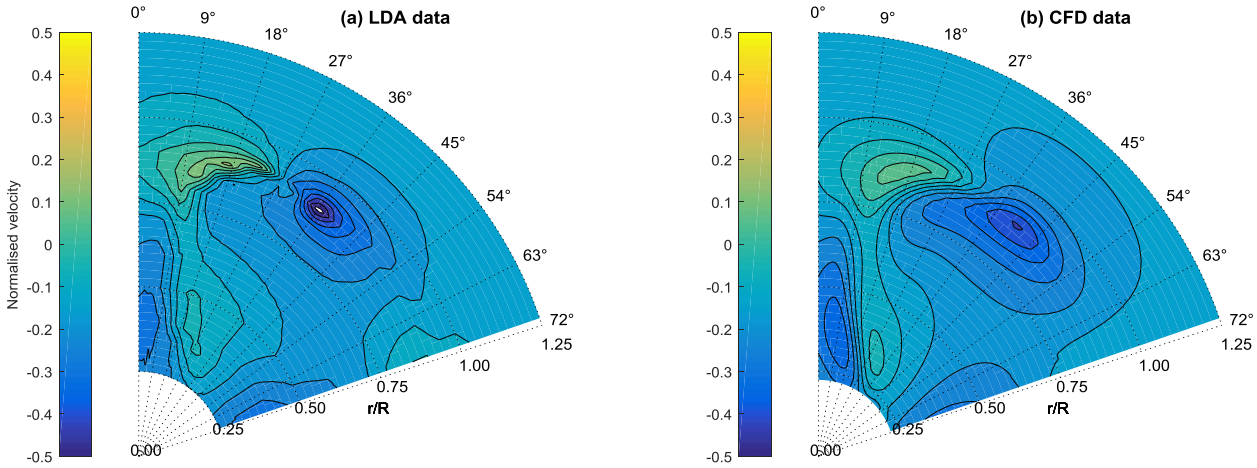

Figure 15: Comparison of polar contour plots of radial velocity component over a blade pass at an axial distance, x/D = 1/4